Stabilizing Fluid-Fluid Displacements in Porous Media Through Wettability Alteration

Mathias Trojer, Michael L. Szulczewski, and Ruben Juanes*

Massachusetts Institute of Technology, 77 Massachusetts Avenue, Building 1, Cambridge, Massachusetts 02139, USA

(Received 10 September 2014; revised manuscript received 4 April 2015; published 21 May 2015)

We study experimentally how wettability impacts fluid-fluid-displacement patterns in granular media. We inject a low-viscosity fluid (air) into a thin bed of glass beads initially saturated with a more-viscous fluid (a water-glycerol mixture). Chemical treatment of glass surfaces allows us to control the wetting properties of the medium and modify the contact angle θ from 5° (drainage) to 120° (imbibition). We demonstrate that wettability exerts a powerful influence on the invasion morphology of unfavorable mobility displacements: increasing θ stabilizes fluid invasion into the granular pack at all capillary numbers. In particular, we report the striking observation of a stable radial displacement at low capillary numbers, whose origin lies on the cooperative nature of fluid invasion at the pore scale.

DOI: 10.1103/PhysRevApplied.3.054008

I. INTRODUCTION

Two-phase flow in porous media exhibits a rich variety of fluid-displacement patterns [1–3]. Understanding and controlling these displacements is central to many industrial processes and natural phenomena, including enhanced oil recovery [4], shale gas production [5,6], geological CO_2 storage [7,8], operation of low-temperature polymer-electrolyte fuel cells [9], water infiltration in soil [10], and ink spreading on paper [11].

Immiscible fluid-displacement patterns in porous media have been studied in depth in the drainage regime, that is, when the displacing fluid is less wetting to the porous medium than the displaced fluid. The combined effect of viscous forces, capillary forces, and medium disorder result in patterns that range from viscous fingering (VF) to capillary fingering (CF) to stable displacement [1,2,12–15]. From experimental observations in glass micromodels, this fundamental behavior was mapped out by Lenormand *et al.* [2] on a phase diagram as a function of viscosity contrast M between the fluids and capillary number Ca, which reflects the relative magnitude of viscous-to-capillary forces.

Extensions to the Lenormand diagram have addressed the effects of gravity [16], pore-scale disorder [17,18], fluid compressibility [3,19], the crossover between regimes including the existence of a Ca-dependent crossover length scale [17,18,20–22], and frictional forces between grains leading to a whole new set of displacement patterns [3,23–27]. Yet, this wealth of observations has been restricted to a *drainage* process.

Many experimental observations also exist for *imbibition* in the regime of favorable viscosity contrast—when the invading fluid is more wetting and more viscous than the defending fluid [11]. Much of this work has focused on describing the roughness of the imbibition front in a disordered medium like a porous medium [28–33] or a Hele-Shaw cell with rough surfaces [34–36]. Fundamental observations on pore-scale mechanisms controlling imbibition, such as snap-off and cooperative filling [37] have been incorporated into quasistatic pore-scale models simulating two-phase flow on idealized 2D geometries [38,39] and network representations of porous media [40–43].

In contrast, here we are interested in imbibition in the regime of unfavorable viscosity contrast that favors unstable fluid-fluid displacement: relatively high velocity and high viscosity contrast. Our knowledge and understanding of imbibition in this regime is much less complete, even in simple geometries like a straight capillary tube [44,45] or Hele-Shaw cell [46]. Experiments in transparent porous-media cells illustrating the phenomenon of viscous fingering date back to the 1950s [47,48]. Classic experiments have shown a fundamental difference between imbibition and drainage in terms of the length scale of the instability [14], and have pointed to the associated (and still puzzling) dynamic capillary pressure that accompanies these unstable porous media flows [49]. These observations remain largely unexplained, and thus far inaccessible to both pore-scale and continuum models. A reason for this challenge is, in our view, the importance of nonlocal effects at the front [10,50–52].

From the point of view of engineering applications, there is little doubt that wetting properties play a key role in the extraction of oil and gas from hydrocarbon reservoirs [53–56]. Despite the evidence for the potential of wettability alteration as an agent for enhanced oil recovery (including low-salinity water flooding [57], surfactant flooding [58–60], and thermal stimulation [61]), the complex physics of wetting continue to challenge our fundamental understanding of the mechanisms that link surface

*juanes@mit.edu

chemistry with the fluid dynamics of multiphase flow at the pore and reservoir scales.

Here we perform a systematic experimental study of the impact of wetting properties on the fluid-fluid invasion morphology in porous media. We effectively extend Lenormand's diagram to elucidate the impact of wetting properties (as measured by contact angle) on the displacement pattern for highly unfavorable viscosity ratios. We find that, as the invading fluid becomes more wetting, the invasion front becomes more compact and more effectively sweeps the defending fluid at all capillary numbers—both in the viscous-fingering and capillary-fingering regimes. Our main results are a visual phase diagram of the displacement pattern as a function of capillary number and contact angle, and a quantitative analysis of the dependence of the emerging length scale on the wetting properties of the system.

II. EXPERIMENTAL SETUP

We conduct two-phase fluid-displacement experiments in a radial Hele-Shaw cell packed with glass beads. The radial cell consists of a base, a frame, and a lid, all made of soda-lime glass (Fig. 1). The beads are also made of soda-lime glass. The experimental setup is described in detail in Appendix A. The bead matrix is initially fully saturated with a viscous mixture of water and glycerol ($\eta_{\mathrm{liq}} = 5.83$ cP), placed by slow injection through the injection port. This initial fluid is displaced by injecting air ($\eta_{\mathrm{air}} = 0.018$ cP) at rate Q which is held constant throughout each individual experiment ($Q = 170$, 17.0, 1.70, and 0.170 ml/ min). The viscosity contrast between these two fluids is $M = \eta_{\mathrm{liq}}/\eta_{\mathrm{air}} \approx 320$—in the regime of

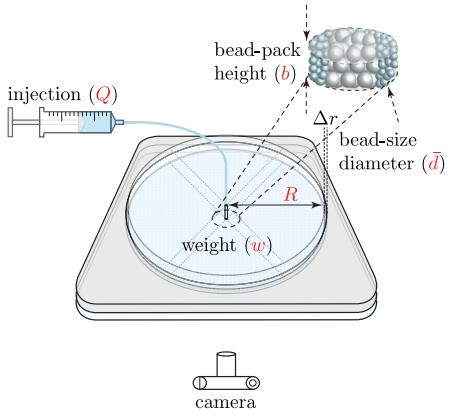

FIG. 1. Experimental setup: a thin glass bead pack (nominal bead-size diameter $\bar{d} \approx 490$ μm) of height b of 5–7 beads is confined in between the bottom and top lid of a radial Hele-Shaw cell of radius $R = 10.6$ cm (a confinement weight $w = 18$ kg rests on top of the lid). Air is injected from the top at a fixed rate Q to displace a water-glycerol mixture that fills the cell initially. Time-lapse images are taken with a camera placed underneath the cell.

highly unfavorable mobility ratios we are interested in. We study how the invasion morphology changes with the wetting properties by treating the cell and the glass beads using chemical vapor deposition (CVD) of silane-based substances, to achieve specific contact angles θ to water-glycerol mixtures ranging from almost perfectly hydrophilic to hydrophobic ($\theta \approx 5°$, 20°, 60°, 90°, 120°) (see Appendix A). We ensured reproducibility of the results by repeating each experiment three to five times.

III. EXPERIMENTAL RESULTS

To rationalize the results, we first define an effective capillary number Ca^* that reflects the balance between viscous and capillary forces at the scale of the entire cell as the ratio between a characteristic capillary pressure difference for invasion along the displacement front, δP_c, and the characteristic viscous pressure loss across the cell in the direction perpendicular to the front, δP_v [18,27]. From simple arguments using the classical Laplace pressure and Darcy's law, we propose the scaling $\delta P_c \sim \gamma/r_{\mathrm{min}} - \gamma/r_{\mathrm{max}} \sim \gamma/d$, and $\delta P_v \sim (\eta_{\mathrm{liq}} QR)/(\gamma b d^3)$, leading to

$$\mathrm{Ca}^* = \frac{\eta_{\mathrm{liq}} QR}{\gamma b d^2}. \tag{1}$$

This dimensionless number is necessarily a crude representation of the balance between the viscous and capillary forces, because this balance changes over the course of an experiment in a radial system. Also, intentionally, this number does not account for the wetting properties of the system. As we contend below, these effects cannot be subsumed into an effective capillary number.

Our main result is a visual phase diagram of the invasion morphology of air displacing the water-glycerol mixture, as a function of Ca^* and contact angle θ (Fig. 2). Shown are the displacement patterns at the end of the experiment, when the injected fluid breaks through the perimeter of the cell.

The leftmost column ($\theta = 5°$) corresponds to the well-known drainage regime. At low Ca^*, we observe capillary fingering, characterized by intermittent air-water displacements that produce an overall asymmetric pattern. At high Ca^*, we observe viscous fingering, characterized by continuous air-water displacements that produce a more radially symmetric pattern. Virtually identical morphologies are observed for slightly less wetting conditions to the liquid ($\theta = 20°$). While the transition between the morphologies is gradual, qualitatively comparing the pattern symmetry and invasion rate (continuous vs intermittent) suggests that the VF-CF transition occurs at an effective capillary number of order one, suggesting that our definition of Ca^* in Eq. (1) is valid.

Wetting properties exert a remarkable control on the fluid displacement at both high and low capillary numbers. At high capillary numbers (bottom two rows, $\mathrm{Ca}^* = 50$, 5),

altering the wetting properties of the substrate towards imbibition (less wetting defending fluid) results in a gradual stabilization of the viscous-fingering displacement. In strict drainage ($\theta = 5$, 20°), VF is a pore-scale instability: the fingers of the invading fluid have a characteristic thickness equal to the pore size of the granular pack (see Video 1 [62]). This characteristic length scale changes as the invading fluid is more wetting ($\theta = 90$, 120°), resulting in fingers whose thickness is clearly larger than the pore scale (see Video 2 [62]). This fundamental observation dates back to linear-displacement experiments in the 1980s [14], where the emphasis was on reporting and understanding the dependence of the emerging length scale on the capillary number [49], rather than the transition from drainage to imbibition.

In Fig. 2 we report a remarkable finding, which had heretofore remained elusive to direct observation: the complete stabilization of unfavorable mobility-ratio displacements in the regime of low capillary numbers, as a result of wettability alteration (top two rows, $\mathrm{Ca}^* = 0.5$, 0.05). Fluid invasion becomes a perfectly stable, radial, outward-growing displacement—which maximizes sweep of the initial fluid—as the invading fluid is more wetting to the substrate.

While this is not visible from the single snapshots in Fig. 2, the growth activity of the displacement front is also heavily mediated by the wetting properties. In particular, the displacement in the drainage CF regime consists of a sequence of avalanches, whose size distribution has been well characterized [63] and whose origin has been assimilated to well-known statistical growth models [15]. This intermittent pattern growth leaves much of the displacement front frozen during invasion (see Video 3 [62]).

In contrast, we find that low-Ca^* imbibition leads to a smooth, uniform, simultaneous advancement of the displacement front (see Video 4 [62]). We interpret this feature as the macroscopic consequence of the strong cooperative nature of fluid invasion at the pore scale during imbibition [37–39,64]. In imbibition, due to the shape of the fluid-fluid menisci between grains, invasion past a pore throat often occurs when neighboring menisci touch; this leads to an unstable fluid-fluid interface that advances to adopt a stable configuration. Therefore, loosely speaking, invasion at one pore "pulls" the interface at neighboring pores, in contrast with the prototypical slow-drainage regime—in which invasion can be considered at each pore independently. This nonlocal fluid invasion in imbibition has been illustrated in simple geometries by means of simulations of point injection [39] and experiments of multiphase lock-exchange flows in porous media [64,65]. This strong nonlocal effect along the wetting front has been interpreted in the past as a macroscopic surface tension [49] and, more recently, it has led to the formulation of phase-field models of multiphase flow in porous media [10,66].

IV. QUANTITATIVE ANALYSIS

To gain quantitative insight into the visual trends observed experimentally, we first compute the evolution of the invaded area A_{inv} as a function of radial distance r using the box-counting method. Taking the final snapshot for each experiment in Fig. 2, we confirm a power-law relation $A_{\mathrm{inv}} \sim r^{D_f}$ over almost a decade of data, where D_f is the fractal dimension [1,2]. The impact of Ca^* and θ on D_f is shown in Fig. 3(a). For strict drainage displacements ($\theta = 5°$), the system displays a transition from $D_f \approx 1.72$ at

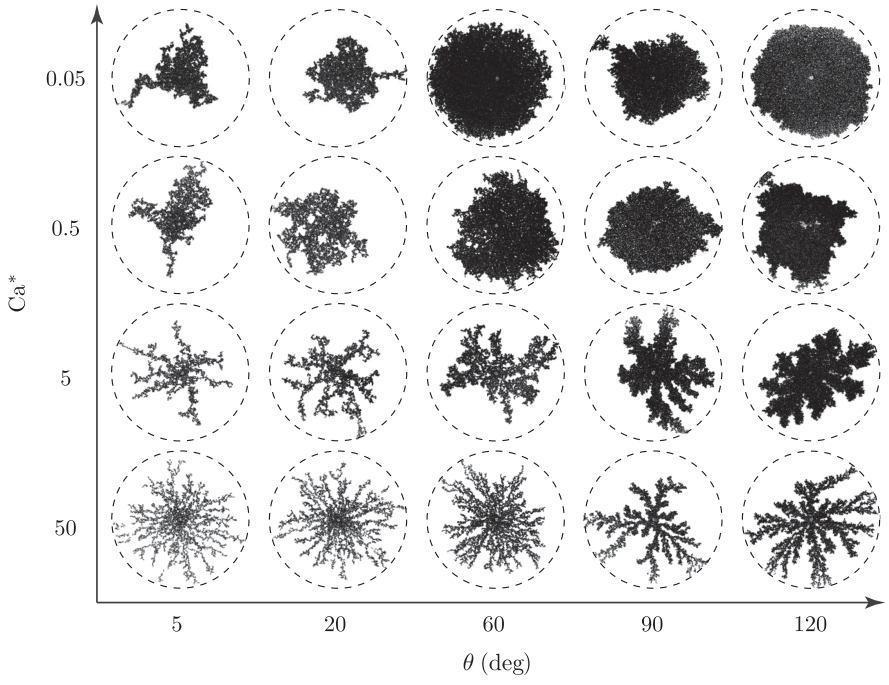

FIG. 2. Visual phase diagram of the fluid-fluid-displacement morphologies obtained during air injection (dark) into a porous medium filled with a mixture of water and glycerol (clear), as a function of the effective capillary number Ca^* [Eq. (1)] and the static contact angle θ ranging from strict drainage ($\theta \approx 5°$) to forced imbibition ($\theta \approx 120°$). The viscosity contrast between the fluids is $M = \eta_{\mathrm{liq}}/\eta_{\mathrm{air}} \approx 320$.

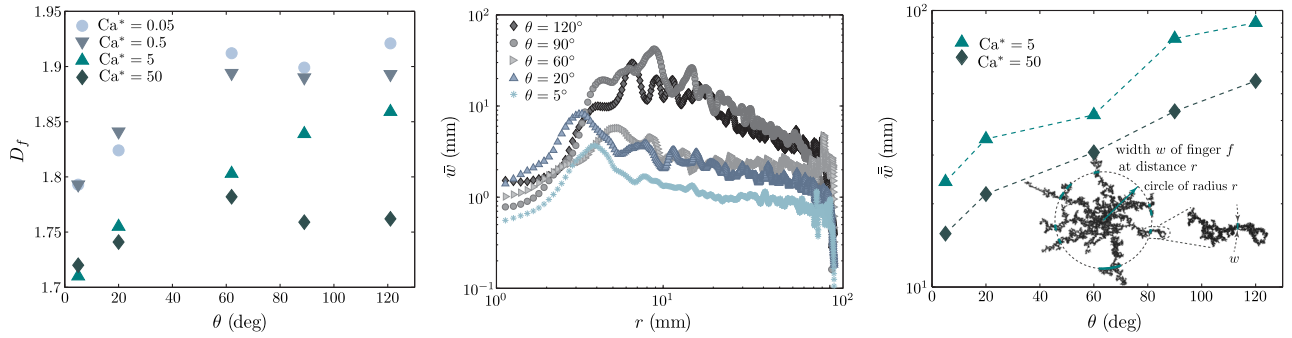

FIG. 3. (a) Fractal dimension D_f vs static contact angle θ for all single-frame snapshots presented in Fig. 2, computed using the box-counting method. (b) Average finger width $\bar{w}$ vs radial distance r, for $\mathrm{Ca}^* = 50$ and all different contact angles. (c) Effective finger width $\bar{\bar{w}}$ vs static contact angle θ in the viscous-fingering regime ($\mathrm{Ca}^* = 5$ and 50); the monotonically increasing trend confirms quantitatively the stabilizing effect of wetting to the invading fluid. Inset: schematic illustrating the computation of the average finger width $\bar{w}$ at any given radial distance r.

high Ca^* to $D_f \approx 1.8$ at low Ca^*, a trend that is consistent with previously reported fractal dimensions for VF and CF in drainage [63], corresponding to classical statistical-physics models: diffusion-limited aggregation [12,67], and invasion percolation [15], respectively. The stabilization of the invasion pattern as a result of wettability alteration is apparent from the increasing trend in D_f as a function of θ at all capillary numbers. At low Ca^*, $D_f \approx 1.9$ for $\theta \geq 60°$, indicative of very compact displacement. At a high capillary number ($\mathrm{Ca}^* = 50$), however, the fractal dimension does not capture the stabilization of the displacement with the contact angle evidenced in the experiments (Fig. 2, bottom row). This is because, even though the fingers are wider, the displacement does not involve a "core" of more complete filling of the injected fluid.

A more relevant measure of the stabilizing effect of imbibition in the viscous-fingering regime at high Ca^* is finger width [14,49]. For each displacement experiment, we determine the average finger width $\bar{w}$ at the end of injection as a function of radial distance r [see the inset in Fig. 3(c)]. We report the curves $\bar{w}(r)$ for experimental conditions in the viscous-fingering regime ($\mathrm{Ca}^* = 5$), and for all contact angles [Fig. 3(b)]. First, we find a clean trend of $\bar{w}$ as a function of distance: beyond $r = 10$ mm, the average finger width decreases slightly with r. We define an effective finger width $\bar{\bar{w}}$ for each experiment by further averaging finger width between $r = 10$ and 80 mm. The effective finger width of the set of fluid-fluid displacements in the viscous-fingering regime exhibits a robust, monotonically increasing trend as a function of contact angle [Fig. 3(c)], illustrating clearly the stabilizing effect of imbibition with respect to drainage.

V. DISCUSSION AND CONCLUSIONS

In summary, we report experiments that elucidate the impact of wetting properties on the morphology of fluid-fluid displacement in porous media, in the regime of highly unfavorable viscosity contrast—when the injected fluid is much less viscous than the initial defending fluid. Our work therefore extends the classical Lenormand diagram [2] to account for the dependence of fluid invasion on wetting properties.

Our experimental investigation focuses on the dependence of the viscous-fingering length scale on wettability—which is made possible by achieving detailed control of the wetting properties of the system (see Appendix A). As such, it complements earlier investigations focused on the dependence of the viscous-fingering length scale on capillary number [14,49]. We demonstrate the stabilizing effect of wettability as the system transitions from drainage to imbibition—that is, as the porous medium is more wetting to the invading fluid. At high capillary numbers, this is best evidenced by the broadening of viscous fingers in imbibition versus drainage [Fig. 2, bottom two rows; Fig. 3(c)]. At low capillary numbers, our experiments provide evidence of the stabilization of fluid invasion during imbibition, even for extremely unfavorable viscosity contrast. In general, the instability is delayed by the effect of wetting, and develops at a higher value of the capillary number. This result bears important implications for enhanced oil recovery and, in particular, for the design of water flooding in heavy oil reservoirs [68].

Our experimental investigation and quantitative analysis of invasion morphologies open up the intriguing possibility of a dynamic scaling analysis, that is, a temporal analysis of the morphology of the displacement front in the spirit of Family-Vicsek models of surface growth [63,69], which has recently been applied to circular geometries [70]. Perhaps more importantly, they also point to the need for the development of a mechanistic model at the pore scale, and a macroscopic model at the continuum scale, that capture the nonlocal effects of wettability on the *dynamics* of multiphase flow in porous media, including viscous-driven and gravity-driven unstable flows [10,14,49], and capillary fracturing of granular media [27,71].

ACKNOWLEDGMENTS

We gratefully acknowledge financial support for this work, provided by Eni S.p.A. and by the ARCO Chair in Energy Studies.

APPENDIX A: EXPERIMENTAL SETUP AND WETTABILITY ALTERATION

The experimental apparatus consists of a radial Hele-Shaw cell packed with glass beads. The radial cell consists of a base, a frame, and a lid (see Fig. 1). The base is made of a square piece of soda-lime glass. The frame is made of a square piece of 1-cm-thick acrylic with a circular hole of radius $R = 10.65$ cm cut out. The frame is epoxied on top of the base and provides lateral confinement for the glass bead pack that occupies the hole. The circular lid is made of 2-cm-thick soda-lime glass and fits into the hole, providing vertical confinement for the bead pack. The radius of the lid is approximately 10.30 cm, which makes the gap between the lid and the frame large enough to allow fluid to escape freely, but small enough to prevent the outflow of glass beads. The lid has a 1.5-mm hole drilled in the center through which fluids are injected into the cell.

The bead pack is made of nonsintered, soda-lime glass beads. The beads have a mean diameter of $\bar{d} \approx 490$ μm; their size distribution is shown in Fig. 4(a). To compose the pack, we first place a 2-mm-thick, coarse mesh into the cell to provide a reference height for packing. The mesh is a regular square lattice, except at the center where there is a small circular hole [Fig. 4(b)]. We distribute 60 ml of beads uniformly into the mesh, except in the center hole, which we fill with larger beads of diameter $d_c = 1$ mm. When the beads evenly fill all the mesh compartments, we carefully remove the mesh to minimally disturb the pack, and then weakly vibrate the cell laterally by tapping on it. This homogenizes the pack. We then place the glass lid on top of the pack and tap the cell a few more times to ensure the lid fits tightly on top of the beads. The final height of the pack is slightly smaller than the thickness of the mesh since the vibrations slightly reduce the overall pack volume. This packing procedure creates a homogeneous permeability and porosity throughout the bead pack.

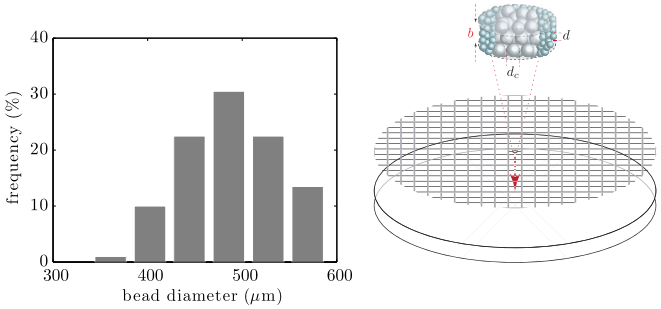

FIG. 4. (a) Bead-size distribution of MO-SCI GL0191B4/425-600SC soda-lime spheres used to create the solid porous matrix; the measured mean average bead-size diameter of 200 representative individual spherical beads is $\bar{d} = 488$ μm. (b) Regular square lattice initially placed in the circular hole cut to maintain reproducibility of bead-pack height b, porosity, and permeability of individual experiments.

The bead matrix is initially fully saturated with a viscous mixture of water and glycerol, placed by slow injection through the injection port. We always confirm uniformity of the packing by observing a circular invasion of this viscous liquid. To displace the initial fluid, we inject air at rate Q, which is held constant throughout each individual experiment. The viscosity contrast between these two fluids is $M = \eta_{\text{liq}}/\eta_{\text{air}} \approx 320$. To allow a clear view on the transparent porous matrix, pictures are taken from the bottom of the Hele-Shaw cell with a digital single-lens reflex (SLR) camera (Canon EOS 1D) as well as with a Complementary Metal Oxide Silicon (CMOS) monochrome Universal Serial Bus (USB) camera (maximum frame rate of 30 fps). We use the high-resolution pictures obtained with the SLR camera for image processing of the final pattern before breakthrough of the invading fluid through the edges of the cell. Light-emitting-diode light panels illuminate the setup from all sides to ensure picture quality.

As our interest focuses specifically on the impact of wetting properties on the invasion morphology, the Hele-Shaw cell and the glass beads are chosen to be made out of the exact same material: soda-lime glass. The wetting properties of soda-lime glass are modified to either become almost perfectly hydrophilic (contact angle of the water-glycerol mixture in the presence of air $\theta \approx 5°$) or hydrophobic ($\theta \approx 120°$). To ensure cleanliness of the substrate before altering wettability, we use a liquid-chemical acid mixture to attack and remove any impurities on the glass surfaces. Rinsing with highly purified water, the substrate is

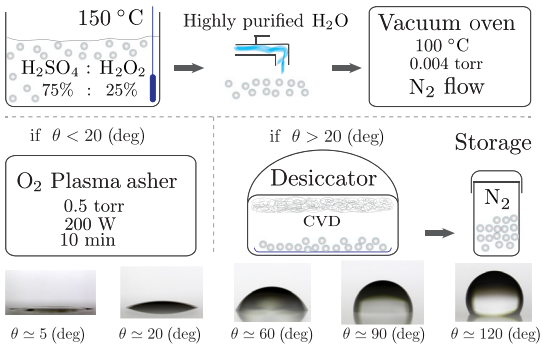

FIG. 5. Wettability alteration on soda-lime glass using chemical vapor deposition (CVD). The silanization procedure is tuned to achieve the desired wetting properties for five different contact angles with respect to the viscous water-glycerol mixture and air: (1) $\theta = 5° \pm 1.2°$, O_2 plasma asher; (2) $\theta = 20° \pm 0.8°$, no CVD treatment; (3) $\theta = 62° \pm 1.8°$, dichlordimethylsilan, 5% in a vacuum oven at 150 °C; (4) $\theta = 89 \pm 0.8°$, dichlordimethylsilan, 5%; (5) $\theta = 121 \pm 2.3°$, (tridecafluoro-1,1,2,2-tetrahydrooctyl)-1-trichlorosilane.

let dry in an vacuum oven at 60 °C by flushing the vacuum chamber with gaseous N_2. An O_2 plasma asher is applied on the dry substrate (glass beads) as well as on the Hele-Shaw cell to obtain hydrophilic conditions where in case of an hydrophobic surface treatment, silane-based substances are applied using CVD to homogeneously modify wettability of the experimental solid framework (Fig. 5).

APPENDIX B: INVASION DYNAMICS

The dynamics of the fluid-fluid displacement in the different invasion regimes are demonstrated by videos from sequences of images taken during air injection. Each image is obtained by subtracting the initial image prior to air invasion. Air shows as white, and water and beads show as black (see Supplemental Material [62]).

Video 1: Viscous fingering in drainage.—Experimental conditions: $Q = 170$ ml/ min, $\theta = 5°$. The length scale of the instability is the pore scale. The video is in real time.

Video 2: Viscous fingering in imbibition.—Experimental conditions: $Q = 170$ ml/ min, $\theta = 120°$. The change in wetting properties leads to thicker fingers compared to those of Video 1. The video is in real time.

Video 3: Capillary fingering in drainage.—Experimental conditions: $Q = 0.170$ ml/ min, $\theta = 5°$. Intermittent propagation of the air-liquid interface, advancing at alternating locations. The final pattern is asymmetric, with thick, dense fingers. Video speedup of 60.

Video 4: Stable displacement in imbibition.—Experimental conditions: $Q = 0.170$ ml/ min, $\theta = 120°$. Smooth, uniform, simultaneous advancement of the displacement front, as a macroscopic consequence of the strong cooperative nature of fluid invasion at the pore scale. Video speedup of 230.

[1] K. J. Måløy, J. Feder, and T. Jøssang, Viscous Fingering Fractals in Porous Media, Phys. Rev. Lett. **55**, 2688 (1985).

[2] R. Lenormand, E. Touboul, and C. Zarcone, Numerical models and experiments on immiscible displacements in porous media, J. Fluid Mech. **189**, 165 (1988).

[3] B. Sandnes, E. G. Flekkøy, H. A. Knudsen, K. J. Måløy, and H. See, Patterns and flow in frictional fluid dynamics, Nat. Commun. **2**, 288 (2011).

[4] F. M. Orr, Jr. and J. J. Taber, Use of carbon dioxide in enhanced oil recovery, Science **224**, 563 (1984).

[5] T. Patzek, F. Male, and M. Marder, Gas production in the Barnett Shale obeys a simple scaling theory, Proc. Natl. Acad. Sci. U.S.A. **110**, 19731 (2013).

[6] L. Cueto-Felgueroso and R. Juanes, Forecasting long-term gas production from shale, Proc. Natl. Acad. Sci. U.S.A. **110**, 19660 (2013).

[7] IPCC, *Special Report on Carbon Dioxide Capture and Storage*, edited by B. Metz *et al.* (Cambridge University Press, Cambridge, England, 2005).

[8] M. L. Szulczewski, C. W. MacMinn, H. J. Herzog, and R. Juanes, Lifetime of carbon capture and storage as a climate-change mitigation technology, Proc. Natl. Acad. Sci. U.S.A. **109**, 5185 (2012).

[9] C. Y. Wang, Fundamental models for fuel cell engineering, Chem. Rev. **104**, 4727 (2004).

[10] L. Cueto-Felgueroso and R. Juanes, Nonlocal Interface Dynamics and Pattern Formation in Gravity-Driven Unsaturated Flow through Porous Media, Phys. Rev. Lett. **101**, 244504 (2008).

[11] M. Alava, M. Dubé, and M. Rost, Imbibition in disordered media, Adv. Phys. **53**, 83 (2004).

[12] L. Paterson, Diffusion-Limited Aggregation and Two-Fluid Displacements in Porous Media, Phys. Rev. Lett. **52**, 1621 (1984).

[13] J.-D. Chen and D. Wilkinson, Pore-Scale Viscous Fingering in Porous Media, Phys. Rev. Lett. **55**, 1892 (1985).

[14] J. P. Stokes, D. A. Weitz, J. P. Gollub, A. Dougherty, M. O. Robbins, P. M. Chaikin, and H. M. Lindsay, Interfacial Stability of Immiscible Displacement in a Porous Medium, Phys. Rev. Lett. **57**, 1718 (1986).

[15] D. Wilkinson and J. Willemsen, Invasion percolation: A new form of percolation theory, J. Phys. A **16**, 3365 (1983).

[16] Y. Méheust, G. Løvoll, K. J. Måløy, and J. Schmittbuhl, Interface scaling in a two-dimensional porous medium under combined viscous, gravity, and capillary effects, Phys. Rev. E **66**, 051603 (2002).

[17] R. Toussaint, G. Løvoll, Y. Méheust, K. J. Måløy, and J. Schmittbuhl, Influence of pore-scale disorder on viscous fingering during drainage, Europhys. Lett. **71**, 583 (2005).

[18] R. Holtzman and R. Juanes, Crossover from fingering to fracturing in deformable disordered media, Phys. Rev. E **82**, 046305 (2010).

[19] M. Jankov, G. Løvoll, H. A. Knudsen, K. J. Måløy, R. Planet, and R. Toussaint, Effects of pressure oscillations on drainage in an elastic porous medium, Transp. Porous Media **84**, 569 (2010).

[20] J. F. Fernández and J. M. Albarrán, Diffusion-Limited Aggregation with Surface Tension: Scaling of Viscous Fingering, Phys. Rev. Lett. **64**, 2133 (1990).

[21] J. F. Fernández, R. Rangel, and J. Rivero, Crossover Length from Invasion Percolation to Diffusion-Limited Aggregation in Porous Media, Phys. Rev. Lett. **67**, 2958 (1991).

[22] M. Ferer, C. Ji, G. S. Bromhal, J. Cook, G. Ahmadi, and D. H. Smith, Crossover from capillary fingering to viscous fingering for immiscible unstable flow: Experiment and modeling, Phys. Rev. E **70**, 016303 (2004).

[23] B. Sandnes, H. A. Knudsen, K. J. Måløy, and E. G. Flekkøy, Labyrinth Patterns in Confined Granular-Fluid Systems, Phys. Rev. Lett. **99**, 038001 (2007).

[24] C. Chevalier, A. Lindner, M. Leroux, and E. Clement, The instability of slow, immiscible, viscous liquid-liquid displacements in permeable media, J. Non-Newtonian Fluid Mech. **158**, 63 (2009).

[25] X.-Z. Kong, W. Kinzelbach, and F. Stauffer, Morphodynamics during air injection into water-saturated movable spherical granulates, Chem. Eng. Sci. **65**, 4652 (2010).

[26] G. Varas, V. Vidal, and J.-C. Géminard, Morphology of air invasion in an immersed granular layer, Phys. Rev. E **83**, 061302 (2011).

[27] R. Holtzman, M. L. Szulczewski, and R. Juanes, Capillary Fracturing in Granular Media, Phys. Rev. Lett. **108**, 264504 (2012).

[28] M. A. Rubio, C. A. Edwards, A. Dougherty, and J. P. Gollub, Self-Affine Fractal Interfaces from Immiscible Displacement in Porous Media, Phys. Rev. Lett. **63**, 1685 (1989).

[29] R. Lenormand, Liquids in porous media, J. Phys. Condens. Matter **2**, SA79 (1990).

[30] V. K. Horvath, F. Family, and T. Vicsek, Dynamic scaling of the interface in two-phase viscous flows in porous media, J. Phys. A **24**, L25 (1991).

[31] S. V. Buldyrev, A.-L. Barabási, F. Caserta, S. Havlin, H. E. Stanley, and T. Vicsek, Anomalous interface roughening in porous media: Experiment and model, Phys. Rev. A **45**, R8313 (1992).

[32] S. He, G. L. M. K. S. Kahanda, and P. z. Wong, Roughness of Wetting Fluid Invasion Fronts in Porous Media, Phys. Rev. Lett. **69**, 3731 (1992).

[33] M. Dubé, M. Rost, K. R. Elder, M. Alava, S. Majaniemi, and T. Ala-Nissila, Liquid Conservation and Nonlocal Interface Dynamics in Imbibition, Phys. Rev. Lett. **83**, 1628 (1999).

[34] D. Geromichalos, F. Mugele, and S. Herminghaus, Nonlocal Dynamics of Spontaneous Imbibition Fronts, Phys. Rev. Lett. **89**, 104503 (2002).

[35] J. Soriano, J. J. Ramasco, M. A. Rodriguez, A. Hernández-Machado, and J. Ortín, Anomalous Roughening of Hele-Shaw Flows with Quenched Disorder, Phys. Rev. Lett. **89**, 026102 (2002).

[36] J. Soriano, A. Mercier, R. Planet, A. Hernández-Machado, M. A. Rodríguez, and J. Ortín, Anomalous Roughening of Viscous Fluid Fronts in Spontaneous Imbibition, Phys. Rev. Lett. **95**, 104501 (2005).

[37] R. Lenormand, C. Zarcone, and A. Sarr, Mechanisms of the displacement of one fluid by another in a network of capillary ducts, J. Fluid Mech. **135**, 337 (1983).

[38] M. Cieplak and M. O. Robbins, Dynamical Transition in Quasistatic Fluid Invasion in Porous Media, Phys. Rev. Lett. **60**, 2042 (1988).

[39] M. Cieplak and M. O. Robbins, Influence of contact angle on quasistatic fluid invasion of porous media, Phys. Rev. B **41**, 11508 (1990).

[40] M. J. Blunt and H. Scher, Pore-level modeling of wetting, Phys. Rev. E **52**, 6387 (1995).

[41] T. W. Patzek, Verification of a complete pore network simulator of drainage and imbibition, Soc. Pet. Eng. J. **6**, 144 (2001).

[42] P. E. Øren and S. Bakke, Reconstruction of Berea sandstone and pore-scale modelling of wettability effects, J. Pet. Sci. Eng. **39**, 177 (2003).

[43] P. H. Valvatne and M. J. Blunt, Predictive pore-scale modeling of two-phase flow in mixed wet media, Water Resour. Res. **40**, W07406 (2004).

[44] R. Ledesma-Aguilar, A. Hernández-Machado, and I. Pagonabarraga, Theory of Wetting-Induced Fluid Entrainment by Advancing Contact Lines on Dry Surfaces, Phys. Rev. Lett. **110**, 264502 (2013).

[45] L. Cueto-Felgueroso and R. Juanes, Macroscopic Phase-Field Modeling of Partial Wetting: Bubbles in a Capillary Tube, Phys. Rev. Lett. **108**, 144502 (2012).

[46] B. Levaché and D. Bartolo, Revisiting the Saffman-Taylor Experiment: Imbibition Patterns and Liquid-Entrainment Transitions, Phys. Rev. Lett. **113**, 044501 (2014).

[47] P. van Meurs, The use of transparent three-dimensional models for studying the mechanism of flow processes in oil reservoirs, Petrol. Trans. AIME **210**, 295 (1957).

[48] R. L. Chuoke, P. van Meurs, and C. van der Poel, The instability of slow, immiscible, viscous liquid-liquid displacements in permeable media, Petrol. Trans. AIME **216**, 188 (1959).

[49] D. A. Weitz, J. P. Stokes, R. C. Ball, and A. P. Kushnick, Dynamic Capillary Pressure in Porous Media: Origin of the Viscous Fingering Length Scale, Phys. Rev. Lett. **59**, 2967 (1987).

[50] K. J. Måløy, L. Furuberg, J. Feder, and T. Jøssang, Dynamics of Slow Drainage in Porous Media, Phys. Rev. Lett. **68**, 2161 (1992).

[51] L. Furuberg, K. J. Måløy, and J. Feder, Intermittent behavior in slow drainage, Phys. Rev. E **53**, 966 (1996).

[52] L. Xu, S. Davies, A. B. Schofield, and D. A. Weitz, Dynamics of Drying in 3D Porous Media, Phys. Rev. Lett. **101**, 094502 (2008).

[53] P. P. Jadhunandan and N. R. Morrow, Effect of wettability on waterflood recovery for crude-oil/brine/rock systems, SPE Reservoir Eng. **10**, 40 (1995).

[54] J. S. Buckley, Y. Liu, and S. Monsterleet, Mechanisms of wetting alteration by crude oils, Soc. Pet. Eng. J. **3**, 54 (1998).

[55] E. J. Manrique, V. E. Muci, and M. E. Gurfinkel, EOR field experiences in carbonate reservoirs in the United States, SPE Reserv. Eval. Eng. **10**, 667 (2007).

[56] E. J. Spiteri, R. Juanes, M. J. Blunt, and F. M. Orr, Jr., A new model of trapping and relative permeability hysteresis for all wettability characteristics, Soc. Pet. Eng. J. **13**, 277 (2008).

[57] N. Morrow and J. Buckley, Improved oil recovery by low salinity waterflooding, J. Pet. Technol. **63**, 106 (2011).

[58] D. C. Standnes and T. Austad, Wettability alteration in chalk 2. Mechanism for wettability alteration from oil-wet to water-wet using surfactants, J. Pet. Sci. Eng. **28**, 123 (2000).

[59] D. C. Standnes and T. Austad, Wettability alteration in carbonates—Interaction between cationic surfactant and carboxylates as a key factor in wettability alteration from oil-wet to water-wet conditions, Colloids Surf. A **216**, 243 (2003).

[60] P. Chen and K. K. Mohanty, Surfactant-mediated spontaneous imbibition in carbonate rocks at harsh reservoir conditions, Soc. Pet. Eng. J. **18**, 124 (2013).

[61] G. Sharma and K. K. Mohanty, Wettability alteration in high-temperature and high-salinity carbonate reservoirs, Soc. Pet. Eng. J. **18**, 646 (2013).

[62] See Supplemental Material at http://link.aps.org/supplemental/10.1103/PhysRevApplied.3.054008 for videos of the fluid-fluid displacements at different contact angles and capillary numbers.

[63] G. Løvoll, Y. Méheust, R. Toussaint, J. Schmittbuhl, and K. J. Måløy, Growth activity during fingering in a porous Hele-Shaw cell, Phys. Rev. E **70**, 026301 (2004).

[64] B. Zhao, C. W. MacMinn, M. L. Szulczewski, J. A. Neufeld, H. E. Huppert, and R. Juanes, Interface pinning of immiscible gravity-exchange flows in porous media, Phys. Rev. E **87**, 023015 (2013).

[65] B. Zhao, C. W. MacMinn, H. E. Huppert, and R. Juanes, Capillary pinning and blunting of immiscible gravity currents in porous media, Water Resour. Res. **50**, 7067 (2014).

[66] L. Cueto-Felgueroso and R. Juanes, A phase-field model of unsaturated flow, Water Resour. Res. **45**, W10409 (2009).

[67] T. A. Witten, Jr. and L. M. Sander, Diffusion-Limited Aggregation, a Kinetic Critical Phenomenon, Phys. Rev. Lett. **47**, 1400 (1981).

[68] G. P. Willhite, *Waterflooding*, SPE Textbook Series Vol. 3 (Society of Petroleum Engineers, Richardson, TX, 1986).

[69] A. L. Barabási and H. E. Stanley, *Fractal Concepts in Surface Growth* (Cambridge University Press, Cambridge, England, 1995).

[70] K. A. Takeuchi, M. Sano, T. Sasamoto, and H. Spohn, Growing interfaces uncover universal fluctuations behind scale invariance, Sci. Rep. **1**, 34 (2011).

[71] H. Huang, F. Zhang, P. Callahan, and J. Ayoub, Granular Fingering in Fluid Injection into Dense Granular Media in a Hele-Shaw Cell, Phys. Rev. Lett. **108**, 258001 (2012).